

Step-index fibre from metal halide chalcogenide glasses

Julie Carcreff, Pascal Masselin, Catherine Boussard-Plédel, Pierre Kulinski, Johann Troles, David Le Coq

▶ **To cite this version:**

Julie Carcreff, Pascal Masselin, Catherine Boussard-Plédel, Pierre Kulinski, Johann Troles, et al.. Step-index fibre from metal halide chalcogenide glasses. Optical Materials Express, 2020, 10 (11), pp.2800-2812. 10.1364/OME.408334 . hal-03035979

HAL Id: hal-03035979
https://hal.science/hal-03035979

Submitted on 28 May 2021

HAL is a multi-disciplinary open access archive for the deposit and dissemination of scientific research documents, whether they are published or not. The documents may come from teaching and research institutions in France or abroad, or from public or private research centers.

L'archive ouverte pluridisciplinaire **HAL**, est destinée au dépôt et à la diffusion de documents scientifiques de niveau recherche, publiés ou non, émanant des établissements d'enseignement et de recherche français ou étrangers, des laboratoires publics ou privés.

Research Article | Vol. 10, No. 11 / 1 November 2020 / Optical Materials Express 2800
Optical Materials EXPRESS

Step-index fibre from metal halide chalcogenide glasses

JULIE CARCREFF,[1] PASCAL MASSELIN,[2] CATHERINE BOUSSARD-PLÉDEL,[1] PIERRE KULINSKI,[2] JOHANN TROLES,[1] AND DAVID LE COQ[1,*]

[1] Université de Rennes, CNRS, ISCR-UMR 6226, F-35000 Rennes, France
[2] Université du Littoral-Côte d'Opale, LPCA, F-59140 Dunkerque, France
[*] david.lecoq@univ-rennes1.fr

Abstract: The GeS_2-Ga_2S_3 vitreous matrix can incorporate metal halides in its network allowing the properties of the glasses to be adjusted following the composition. In this work, different systems containing either CsCl, CsI, $CdCl_2$, or CdI_2 are investigated in order to determine the compositions having the most suitable properties for drawing a step-index fibre. Indeed, transition glass temperatures and optical parameters such as the optical band-gap, the linear and nonlinear refractive indexes are given. The preforms were prepared using the rod-in-tube technique and multimode step-index fibres were successfully drawn. This initial work led from these glass families, which also show both the possibility to be rare-earth doped and to be permanently photo-written by a femtosecond laser, paves the way to a future mid-IR laser fibre.

© 2020 Optical Society of America under the terms of the OSA Open Access Publishing Agreement

1. Introduction

Glasses transmitting both in the visible and in the infrared (IR) region are potential candidates to lead to the next generation of IR fibres used in many optical application fields. Among the different families of glasses able to fulfil those two transparency conditions, the chalcogenide glasses (ChG) are probably the best candidates [1, 2, 3]. Moreover, the characteristic temperatures and viscosity profiles of ChG are suitable to draw fibre [4, 5] or to mould lenses [6]. Indeed, the potential of ChG fibres has already been demonstrated in many applications, whether in the medical [7, 8] or civil [9, 10] domains. Obviously, it is well-known that the performances of silica fibres up to 3 µm are the best ever reported with losses less than 0.2 $dB.km^{-1}$ [11, 12]. But the mid-IR range beyond 3 µm is not achievable for silica fibres whereas ChG fibres are necessarily good candidates even if the optical losses remain around 0.2-0.5 $dB.m^{-1}$ in the 3-10 µm range [13, 14, 15]. ChG present other advantages since they show a large third-order optical non-linear susceptibility and high index of refraction [16, 17, 18]. Active optical functions are also expected, especially with the development of mid-IR fibre lasers at wavelengths that do not exist yet [19, 20] even if the luminescence at different wavelengths have been already demonstrated [21, 22]. To carry out this ambitious project, it is necessary, firstly, to design step-index fibre in which the core could be rare-earth doped, and secondly to inscribe Bragg mirrors to create a laser cavity [23]. In this work, we focus on the fabrication of the step-index fibre, which could be rare-earth doped and photo-inscribed by femtosecond laser in a close future. The first point requires the presence of gallium (Ga) in the composition of the glass since it facilitates the incorporation of rare-earth ions [24]. Next, the transparency condition in the visible is solved by using sulphur (S) as chalcogenide element rather than selenium or tellurium from which the synthesized glasses are dark or black. This condition is also motivated by the necessity of absence of linear absorption at the writing laser wavelength (actually 800 nm) during the future inscription of Bragg gratings [25]. The photoinscription of photonic structures, by locally modifying the refractive index of sulphide glasses, by means of femtosecond laser is now well controlled [26, 27, 28]. Furthermore,

#408334 https://doi.org/10.1364/OME.408334
Journal © 2020 Received 25 Aug 2020; revised 13 Sep 2020; accepted 13 Sep 2020; published 9 Oct 2020

Optical Materials EXPRESS

in addition to S and Ga elements, germanium (Ge) is a key element to ensure better mechanical properties for the synthesized glasses [29]. In conclusion, the system based on Ge-Ga-S elements is very appropriate for the future considered applications and more particularly, the pseudo-binary system GeS_2-Ga_2S_3 presents a particular interest [30, 31].

The two main possibilities to adjust the properties of the ChG based on the glass matrix GeS_2-Ga_2S_3 consist either in playing with the Ge/Ga ratio or in addition of a metal halide [32]. In this paper, we focus on the $[GeS_2]_{0.80}[Ga_2S_3]_{0.20}$ matrix because we have clearly established the structural consequences of the laser irradiations inside this bulk [33] and successfully inscribed waveguides with or without CsCl [25,28,33]. In consequence, the investigations have been led by adding either CsCl, CsI, CdI_2 or $CdCl_2$ in this glass matrix. Several percentages of metal halide up to 20% were added to widen the choice of potential glasses for the fibre. Next, the possibilities to achieve a step-index fibre are multiple [34] and we have focused on the more adapted technique for the investigated glasses. Thus, the preform was produced by following three steps. The first one is the preparation of the core rod by hot drawing and the second one is the obtention of the cladding tube by a mechanical drilling. The third one consists in the introduction of the core rod into the cladding tube before the drawing [35]. The attenuation measurement of the step-index fibre drawn in this study are then presented.

2. Experimental procedures

The glasses are synthesized from pure metallic elements Ga (7N, Alfa Aesar), Ge (5N, Umicore), S (5N, Sterm) and from the metal halide powder, CsCl, CdI_2, CsI, or $CdCl_2$ (4N, Alfa Aesar). Once a vacuum of 10^{-6} Torr is reached inside the experimental set-up, it is sealed and a complementary distillation of S at 250°C is implemented. The condensation of S takes place in a silica ampoule containing all other elements and compounds. The synthesis is carried out by progressively melting the sealed silica tube containing the elements up to 850°C in a rocking furnace. After a few hours of homogenization, the mixture is quenched in water at room temperature and then, to reduce the internal stresses, the glass is annealed below the glass transition temperature (T_g), T_g - 15°C, for 4 hours before a slow cooling down to room temperature [36]. The glass rods thus obtained were either cut and polished into pellets 2 mm thick and 10 mm diameter in order to carry out different characterizations, or used to elaborate the fibres.

In order to observe the influence of the halogen elements in the $[GeS_2]_{0.80}[Ga_2S_3]_{0.20}$ matrix, the thermal properties were measured with a Differential Scanning Calorimetry (DSC Q20 Thermal Analysis). The temperature ramp was set at 10°C.min^{-1} in order to measure both the onset glass transition temperature (T_g) and the onset crystallization temperature (T_x) of the sample. The density was determined by the Archimedes' principle using a Mettler Toledo XS64 balance and the water as immersion fluid.

The optical properties of the glass were measured on 2mm-thickness glass sample. The refractive indices of each sample have been measured by using a prism coupling method at 825 nm, 1311 nm and 1551 nm (Metricon [37]).

The transmissions of glasses in the visible and near infrared ranges were measured using a Perkin Elmer double beam spectrophotometer and a Bruker Fourier transform infrared (FTIR) spectrophotometer (Tensor 37), respectively.

The nonlinear optical properties were measured by the Z-scan method. The excitation was provided by a Ti:sapphire regenerative amplifier (RegA from Coherent Inc.) delivering 350 fs pulses of central wavelength $\lambda = 800$ nm at a repetition rate of 10 kHz. A 150 mm focal length lens was used to focused to beam on the samples of 2 mm thickness. A first photodiode was placed before the sample in order to record a reference signal. After the sample the beam was separated into two part to measure simultaneously the nonlinear absorption and the nonlinear refractive index. A diaphragm with transmission $S = 0.4$ was placed on the beam path for the measurement of the nonlinear refractive index n_2.

Optical Materials EXPRESS

The nonlinear absorption curve was fitted to the formula:

$$T(z, S = 1) = \sum_{m=0}^{\infty} \frac{(-q_0(z, t = 0))^m}{(m + 1)^{3/2}} \quad (1)$$

where : $q_0(z, t) = \frac{A}{(1+z^2/z_R^2)}$. In this formula, z_R is the Rayleigh range of the beam and $A = \beta I_0(t) L_{eff}$. L_{eff} is the effective length that takes into account the linear absorption α: $L_{eff} = (1 - e^{-\alpha L})/\alpha$.

The expression of the transmission used during the fitting procedure for the determination of n_2 is:

$$T(z, \Delta\Phi_0) = 1 - \frac{4\Delta\Phi_0 x}{(x^2 + 9)(x^2 + 1)} \quad (2)$$

where $x = z/z_R$ and $\Delta\Phi_0 = \frac{2\pi}{\lambda} L_{eff} n_2 I_0$.

The transmission is measured for several values of the irradiance I_0 and the Fig. 1 shows the normalized measurements for the determination of β (Fig. 1-a) and n_2 (Fig. 1-b). The normalization of the n_2 curves includes the nonlinear absorption.

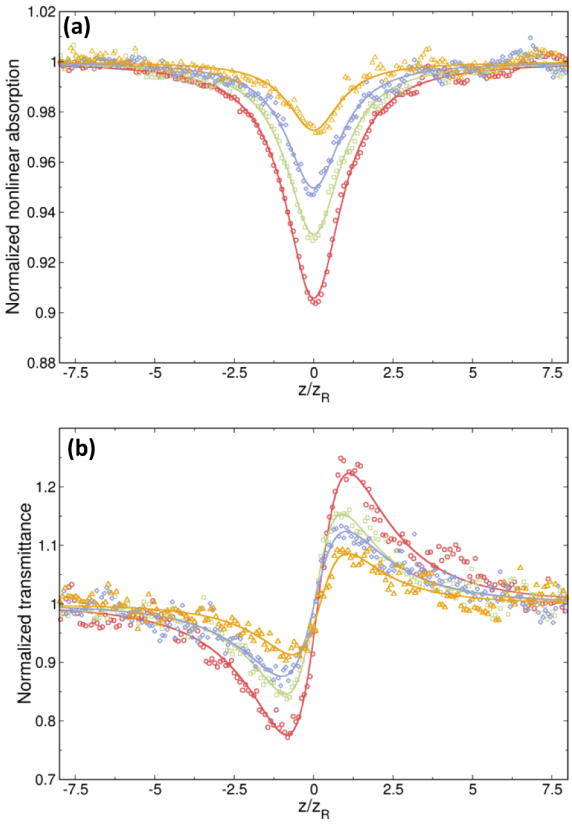


Fig. 1. Typical plots of the nonlinear absorption β (a) and normalized transmittance (b) for different values of the irradiance for glass samples. The data were recorded for the specific composition $([GeS_2]_{0.80}[Ga_2S_3]_{0.20})_{95}$ $(CsCl)_5$.

The dependence of the coefficient A and $\Delta\Phi_0$ with the irradiance was then linearly fitted and the values of β and n_2 were determined from the slope of the lines. An example of these fits is shown in Fig. 2.

All synthetized glass rods used for drawing were thoroughly polished at their surface to remove the slight imperfections. The glass rod corresponding to the core glass is drawn in order to reach

Optical Materials EXPRESS

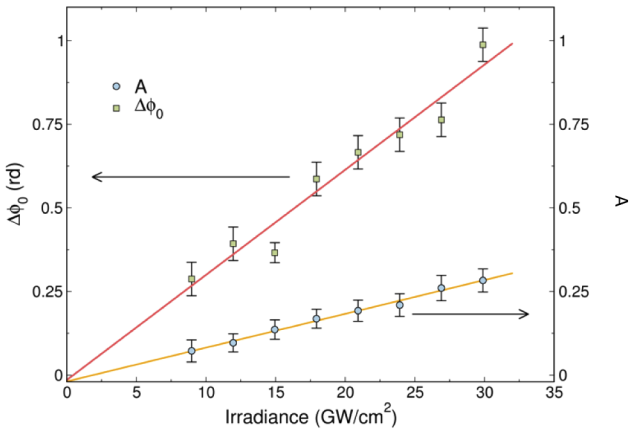


Fig. 2. Dependence of the coefficient A and $\Delta\Phi_0$ with the irradiance and their linear fit. The slopes of the linear fits are used for the determination of β and n_2.

a stick with a 1 to 1.5 mm diameter. The second glass rod, corresponding to the cladding and having a lower linear refractive index was previously drilled mechanically using a drill press (Fig. 3-a&b). A hole of 1 to 1.5 mm diameter was longitudinally produced and then polished to eliminate scratches and imperfections that may appear during drilling. The core rod can then be inserted inside the perforated cladding rod to get the preform of the future step-index fibre (Fig. 3-c) [34]. The lower part of the preform is placed in a tubular furnace connected to a home-made drawing tower specially designed for soft glasses. A flow of He at 1.5 L.min^{-1} creates an inert atmosphere around the preform during the fibering. The furnace is heated to a temperature of around 600°C and under the effect of gravity, a drop forms and falls down, thus generating the optical fibre that is rolled around a drum. The fibre diameter is controlled by the lowering speed of the preform in the furnace associated with the rolling speed of fibre around the drum. A vacuum was applied during the drawing to optimize the quality of the core/clad interface.

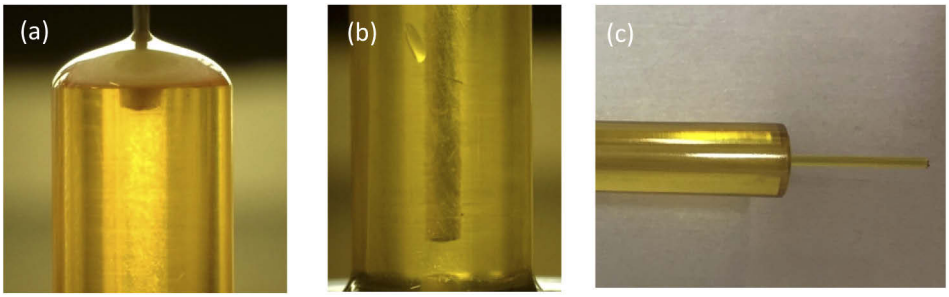


Fig. 3. (a) and (b) Photographs of a $([GeS_2]_{0.80}[Ga_2S_3]_{0.20})_{90}$ $(CsCl)_{10}$ glass rod during mechanical drilling; (c) Photograph of the rod-in-tube preform.

The attenuation measurements of the double index fibre were carried out by means of a FTIR spectrometer (Tensor 37, Bruker) coupled with a MCT detector. In order to remove all the cladding modes an absorbing coating was applied on the surface of the fibre. The cut-back method was used to calculate the attenuation of the fibre core [38] with fibre lengths from 1 m down to 0.20 m. The light signal is injected at the input of the fibre of length L_1 and the measured intensity $I_1(\lambda)$ at the output of the fibre is recorded. The fibre is then cut at the output and a new

Optical Materials EXPRESS

spectrum $I_2(\lambda)$ corresponding to the new length of fibre L_2 is then recorded. The fibre attenuation α (in dB.m^{-1}) as a function of the wavelength λ is determined by using the equation below:

$$\alpha(\lambda) = \frac{10}{L_1 - L_2} log_{10} \frac{I_2(\lambda)}{I_1(\lambda)} \quad (3)$$

3. Glass properties

The possible percentage of incorporation of alkali or transition metal halide under investigations is relatively large in the glass matrix $[GeS_2]_{0.80}[Ga_2S_3]_{0.20}$ since up to 20 mol. % can be added for CsCl, CsI, and CdI_2. This content is only 15 mol. % in case of $CdCl_2$. One can also mention that the stability against ambient humidity becomes a problem for the contents higher than 15 mol.% whatever the metal halide. Some physical (T_g and density) and optical (E_g, n_0, n_2, and β) data collected for all synthesized glasses are reported in Table 1. These families of glass exhibit pretty high T_g for chalcogenide glasses since T_g are between 347°C ($x = 20$ mol. % CsI) and 442 °C (glass matrix).

Whatever the series, T_g decreases with the addition of the metal halide (Fig. 4). This feature is related to the incorporation of the halide elements in the structural network of the glasses, which break the Ge-S or Ga-S bonds, and consequently the crosslinking of the material is reduced. Thus, a modification of the glass structure by opening the tetrahedral structure based on both $GaS_{4/2}$ or $GeS_{4/2}$ occurs. For instance, $Cs^+[GaS_{3/2}Cl]^-$ entities are formed at the end of the chain and the anion leads to a fragmentation of the glass network, which also promotes the formation of glass [39, 40, 41]. Moreover, in those glass families, there are also some 3-fold coordinated S and the addition of halides ensures their disappearance, meaning a decrease of the crosslinking [33, 42].

Unlike T_g, the density of glasses increases when metal halides are added. The density values are around 2.80 g.cm^{-3} without any halide metal and is found, for the highest one, at 3.39 g.cm^{-3} for 20 mol. % of CdI_2 (Table 1). As shown in Fig. 4, the increase of density is more pronounced with the CdI_2 incorporation into the vitreous matrix, which has a higher average atomic mass

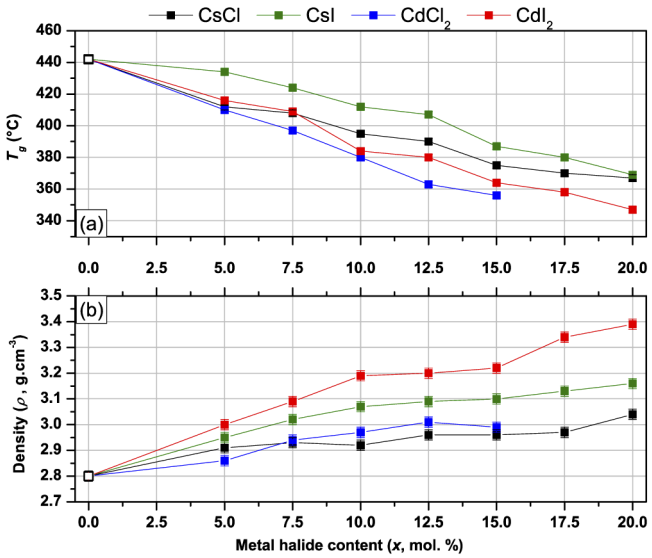


Fig. 4. Evolution of T_g (a) and the density (b) of glasses as a function of the metal halide content in the glass matrix $[GeS_2]_{0.80}[Ga_2S_3]_{0.20}$. The empty symbols represent the data for the glass matrix. The uncertainties on T_g correspond to the height of the symbols.

Optical Materials EXPRESS

Table 1. Tg, density, and optical data for glasses based on the matrix $[GeS_2]_{0.80}[Ga_2S_3]_{0.20}$ in which CsCl, CsI, CdI_2, or $CdCl_2$ are added. (*data at λ = 835 nm from [43])

Metal halide content (mol. %)	T_g (°C) (±2)	Density ($g.cm^{-3}$) (±0.02)	E_g (eV) (±0.02)	n_0 (825 nm) (±0.001)	n_0 (1311 nm) (±0.001)	n_0 (1551 nm) (±0.001)	n_2 (10^{-5} cm^2/GW) (±10%)	β (cm/GW) (±10%)
$[GeS_2]_{0.80}[Ga_2S_3]_{0.20}$								
	442	2.80	2.64	2.151*				
$([GeS_2]_{0.80}[Ga_2S_3]_{0.20})_{100-x}$ $(CsCl)_x$ glasses, $5 \le x \le 20$								
x = 5	412	2.91	2.76	2.105	2.087	2.082	1.62	8.63
x = 7.5	408	2.93	2.76	2.092	2.064	2.059	1.43	8.60
x = 10	395	2.92	2.85	2.071	2.043	2.039	1.52	8.41
x = 12.5	390	2.96	2.88	2.054	2.028	2.023	1.38	6.95
x = 15	375	2.96	2.89	2.038	2.004	2.002	0.97	6.78
x = 17.5	370	2.97	3.00	2.022	1.998	1.993	0.92	6.65
x = 20	367	3.04	3.00	2.000	1.976	1.972	0.88	6.75
$([GeS_2]_{0.80}[Ga_2S_3]_{0.20})_{100-x}$ $(CdI_2)_x$ glasses, $5 \le x \le 20$								
x = 5	416	3.00	2.78	2.139	2.108	2.103	1.68	11.62
x = 7.5	409	3.09	2.77	2.130	2.099	2.094	1.75	12.83
x = 10	384	3.19	2.76	2.126	2.093	2.090	1.76	11.96
x = 12.5	380	3.20	2.76	2.124	2.094	2.088	1.85	11.04
x = 15	364	3.22	2.75	2.116	2.089	2.083	2.13	12.34
x = 17.5	358	3.34	2.75	2.115	2.085	2.080	2.09	11.95
x = 20	347	3.39	2.74	2.108	2.078	2.073	2.08	10.67
$([GeS_2]_{0.80}[Ga_2S_3]_{0.20})_{100-x}$ $(CsI)_x$ glasses, $5 \le x \le 20$								
x = 5	434	2.95	2.82	2.109	2.079	2.075	1.80	6.89
x = 7.5	424	3.02	2.82	2.101	2.072	2.066	1.88	7.87
x = 10	412	3.07	2.83	2.091	2.063	2.057	1.90	7.77
x = 12.5	407	3.09	2.84	2.076	2.047	2.043	1.66	6.70
x = 15	387	3.10	2.86	2.058	2.031	2.026	1.55	7.22
x = 17.5	380	3.13	2.86	2.048	2.021	2.017	1.41	8.03
x = 20	369	3.16	2.87	2.035	2.010	2.005	1.48	8.21
$([GeS_2]_{0.80}[Ga_2S_3]_{0.20})_{100-x}$ $(CdCl_2)_x$ glasses, $5 \le x \le 15$								
x = 5	410	2.86	2.76	2.121	2.093	2.087	1.89	10.59
x = 7.5	397	2.94	2.88	2.110	2.081	2.076	1.71	9.46
x = 10	380	2.97	2.89	2.108	2.079	2.074	1.55	8.47
x = 12.5	363	3.01	2.92	2.101	2.073	2.068	1.49	7.23
x = 15	356	2.99	2.92	2.090	2.063	2.057	1.41	6.55

than the other metal halides. Consequently, the monotonous evolution of density as a function of the metal halide content can be ascribed to their average atomic mass.

The transmission windows for all glasses have been measured in order to extract the electronic band-gap E_g. In Table 1, it is seen that E_g slowly varies versus the content of the metal halide. For instance, in the CsCl- and $CdCl_2$-based glasses, the blue-shift evolution is slightly more pronounced than the CsI- and CdI_2-ones. In addition, the Fig. 5 displays the transmission spectra of the glasses with 10% mol. of metal halide. This percentage has been selected in order to take into account both the chemical stability and the advantage given by a metal halide in the synthesis

Optical Materials EXPRESS

process. The short wavelength cut-off edge of the glasses corresponding to the light to dark yellow colour is located at wavelengths between 420 nm and 450 nm. The inset of the Fig. 5 also shows that glasses with Cl^- ions have a blue shift compared to glasses with I^- ions because of the greater polarizability of Cl^-. It is also seen that the long wavelength cut-off, directly correlated to the phonon energy, is located around 11 µm. In the present case, it is assigned to the intrinsic multiphonon absorptions of Ge–S and Ga–S vibrations [44]. At this level of investigation, the role of the metal halide in the composition is not evidenced.

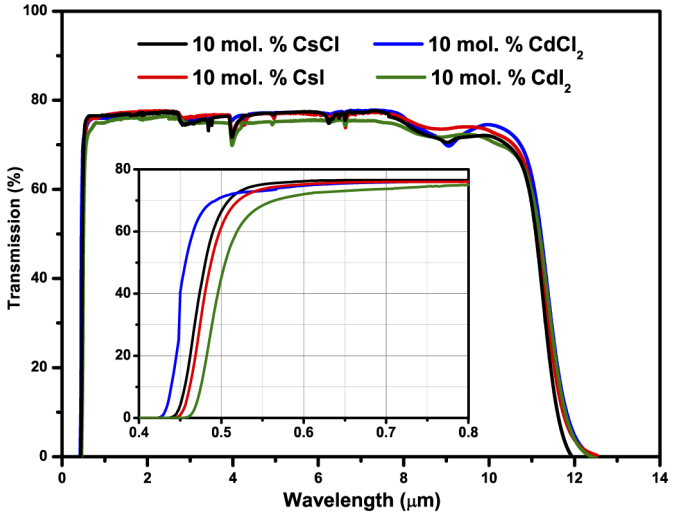


Fig. 5. Vis-IR transmission curves of glass bulks of 1 mm-thickness containing 10% mol. of metal halide. The inset focused on the low-part wavelength to emphasize their visible absorption edge.

Another observation concerns the maximum of transmission for the four samples that is between 75% and 80%. This level of transmission has to be related to the losses by reflexions on the two air-glass interfaces. Moreover, we can observe that the lowest maximum of transmission is found for the CdI_2-based glass. This is consistent with the linear refractive index of the glasses since the CdI_2-based sample possesses the highest n_0, meaning that its reflexion losses will be the highest. The equation of the reflectivity R connects the glass bulk transmission T_0 and the linear refractive index n_0:

$$R = \frac{1 - T_0}{1 + T_0} = \frac{(n_0 - 1)^2}{(n_0 + 1)^2} \tag{4}$$

The transmission spectra reveal also some absorption peaks/bands in the transmission window that are the consequence of presence of impurities in the glass. Thus, the peaks at ~ 2.9 µm, ~ 4.0 µm, ~ 4.9 µm, ~ 6.3 µm, and ~ 6.6 µm are attributed to the vibrations of O-H, S-H, C-S, molecular H_2O, and CS_2, respectively. One can also note a shoulder between 8 µm and 9 µm ascribed to the Ge-O or Si-O bonds, which will be at the origin of the wavelength cut-off of the fibres presented in the next section.

Chalcogenide glasses have high linear refractive indices (n_0) compared to the oxide glasses. The polarizability of the glass constituents is the most influential parameter meaning that n_0 is inevitably higher in the series O < S < Se < Te. Strongly polarizable atoms such as heavy metals also tend to increase n_0 [43]. In our glass series, in which n_0 is around 2 (see Table 1), we clearly observe a decrease of n_0 as a function of the wavelength of measurement corresponding to the normal dispersion. Next, n_0 is also going down if the metal halide content is growing up. The observation of the Fig. 6 leads to assume that (i) the decrease of n_0 versus the halide

Optical Materials EXPRESS

content is more influenced by Cl than by I and (ii) the decrease of n_0 versus the metal content is more influenced by Cs than by Cd. In other words, the variation of n_0 is most important with CsCl additions and less important with CdI_2 additions. Consequently, the intensity of decreasing variation of n_0 as a function of the metal halide content is favored with an electropositive metal and an electronegative halide.

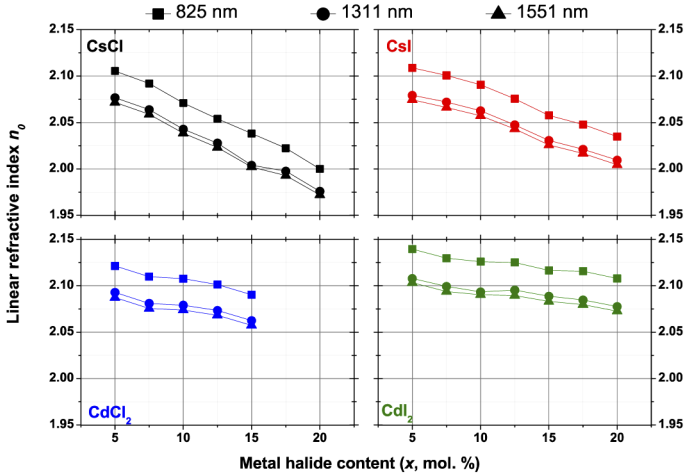


Fig. 6. Evolution of the linear refractive index of glasses at three wavelengths (825 nm (squares), 1311 nm (circles), and 1551 nm (triangles)) as a function of the metal halide content in the glass matrix $[GeS_2]_{0.80}[Ga_2S_3]_{0.20}$. n_0 uncertainties are lower than the height of the symbols.

Chalcogenide glasses are also known to have strong non-linear parameters that is essential for applications in active optic. As stated above, the studied glasses could be involved in future fibre lasers in which the laser cavity will be inscribed by laser writing. It was therefore interesting to

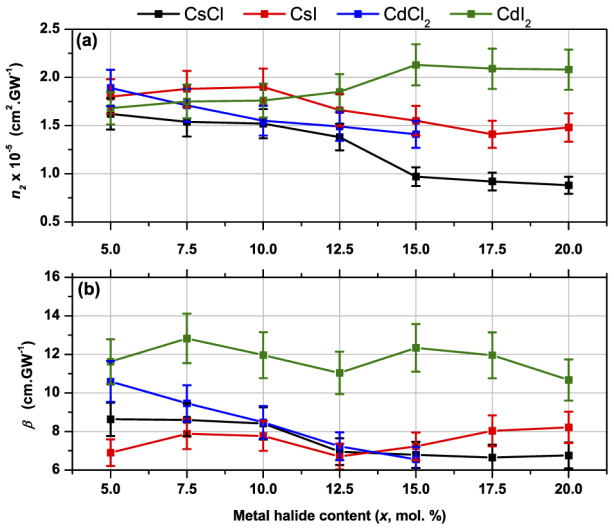


Fig. 7. Evolution of the nonlinear refractive index n_2 (a) and the nonlinear absorption coefficient β (b) of glasses as a function of the metal halide content in the glass matrix $[GeS_2]_{0.80}[Ga_2S_3]_{0.20}$.

Optical Materials EXPRESS

be able to study them over a wide range. The values of the nonlinear refractive index (n_2) and the nonlinear absorption coefficient (β) are given in Table 1. The nonlinear refractive index is around 10^{-14} m^2/W meaning that these values are higher than for silica glasses, which have a nonlinear index of the order of 2.10^{-16} m^2/W at 1.55 µm [45]. Their evolutions with the metal halide additions are plotted in Fig. 7.

Whatever the metal halide the non-linear parameters are going down with metal halide additions. This feature was already pointed out in analogous studies based on $GeS_2 - Ga_2S_3$ with CsCl or CsI glasses [44,18]. It is known that n_2 and n_0 generally show similar behaviour to material polarization. In the investigated series, the addition of halide decreases the lone pair density and consequently its polarizability. The nonlinear absorption coefficient follows the trend of band absorption. Indeed, the nonlinear absorption (mainly two photon absorption in our case) is increasing when the band-gap energy decreases. This behavior is often observed in chalcogenide glasses when the characterization wavelength is slightly lower than $2\lambda_{gap}$, with λ_{gap} is the wavelength associated to the band-gap [46].

4. Fibres and characterisations

Knowing T_g and linear refractive index of the glasses from the 4 series, it is possible to choose different combinations of core/clad compositions. At this preliminary level, the specifications relative to the two compositions were established as follows: (i) $\Delta T_g \leq 20$°C, (ii) $10^{-2} \leq \Delta n_0 \leq 5.10^{-2}$, and (iii) glass compositions of the core and the clad belonging to a unique system. As previously mentioned, the system based on CsCl is intensively studied by our groups in the framework of the photoinscription and the future objectives on the step-index fibres will be in relation with this topic since the inscription of Bragg mirrors inside the core are planned by this technique [25–28]. In consequence, the first attempts of step-index fibre drawing were undertaken with core and clad compositions of $([GeS_2]_{0.80}[Ga_2S_3]_{0.20})_{90}$ $(CsCl)_{10}$ and $([GeS_2]_{0.80}[Ga_2S_3]_{0.20})_{85}$ $(CsCl)_{15}$, respectively. Thus, in the present case, $\Delta T_g = 20$°C, $\Delta n_0 \leq 0.033$ (at 825 nm), and $\Delta T = (T_x\text{-}T_g)$ are 146°C and 164°C for the core and clad glasses, respectively. Unfortunately, our attempts have not been successful since even if some fibres have been drawn, their transmissions were poor. We assume that essentially two reasons are responsible of this failure: ΔT_g is around 20°C between the core and the clad glasses but T_g of the core glass is higher than T_g of the clad glass. This means that during the drawing process the temperature has to be increased sufficiently high to soften the core glass and the consequences on the clad glass could be a bad final contact between the core and clad of the fibre. The other reason concerns the magnitude of Δn_0 that could be higher in order to favour the light injection/propagation in the core of the fibre. In the present case, the infrared light is pretty well transmitted in all the fibre but once an absorbing coating is applied on the clad to empty the cladding modes, no signal is detected at the fibre output.

Consequently, our strategy has been reviewed. The systems with CsI and $CdCl_2$ were eliminated for such application on the basis of experiments. The glasses containing CsI are assumed too fragile since they break more often during the drilling process whereas the glass rods containing $CdCl_2$ are more difficult to synthesize and show a least stability at ambient atmosphere because of their higher hygroscopic behaviour. Next, the CdI_2-based glasses are good candidates from a mechanical point of view, but the decrease of n_0 as a function of the CdI_2 mol. content is weaker than in CsCl-based series. (Table 1). So, the manufacturing of a step-index fibre using a core and a clad from a unique series cannot be considered. Nevertheless, the combination using the two glasses from the CsCl- and CdI_2- based series to produce the step-index fibre is a potential option. In Table 1, we can note that n_0 of the CdI_2-based glasses are higher than the CsCl ones. This feature imposes the CdI_2-based glass as core glass and the CsCl-based one as clad glass. Moreover, within the objectives of the future laser photowriting structure in the core of the fibre,

Optical Materials EXPRESS

the CdI_2-based composition is also appropriate since recent preliminary experiments have been led to a permanent Δn_0 modification under irradiation.

Next, the glass rods have to be synthesized with a relative facility and the risk of crystallization has to be very weak. For the fibering procedure, T_g have to be as close as possible to fit with a single drawing temperature. At last, we give priority to a higher Δn_0 between the core and the clad glasses to force a multimode propagation into the core. Finally, we have chosen to fix the core and the clad compositions as $([GeS_2]_{0.80}[Ga_2S_3]_{0.20})_{90}(CdI_2)_{10}$ and $([GeS_2]_{0.80}[Ga_2S_3]_{0.20})_{90}(CsCl)_{10}$, respectively. Thus, Δn_0 is around 0.055, ΔT_g is 11°C, with a higher T_g for the cladding glass, and ΔT are 120°C and 146°C for the core and clad glasses, respectively. The drawing of this preform was carried out. An image of the cross section the fibre, recorded from a Keyence microscope is depicted in Fig. 8. In the present case the total diameter of the fibre is 300 µm and the core diameter is 35 µm. The core/clad interface does not show any evidence of defects. This observation can probably be liable to an effective polishing of the interior of the cladding tube and a satisfying vacuum configuration during the drawing process.

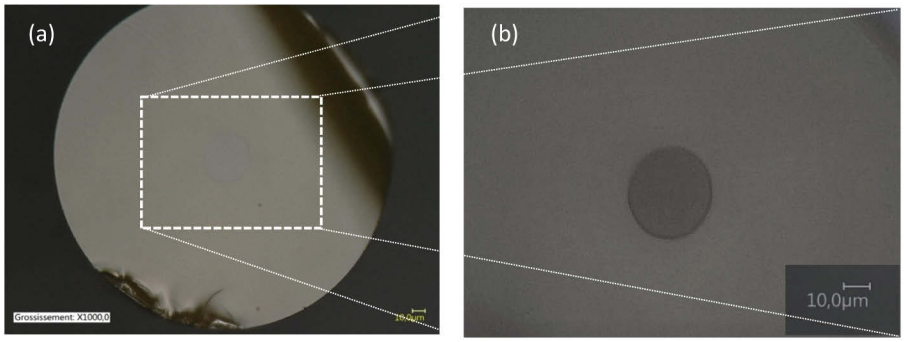


Fig. 8. (a) Microscope image of the cross section of the fibre. The total and the core diameters were measured at 300 µm and 35 µm, respectively; (b) Microscope image zoom on the core/clad interface.

The step-index fibre attenuation, shown in Fig. 9, was measured by means of a FTIR once the clad was emptied of all cladding modes by using an absorbing coating. A comparison of attenuation measurements with a mono-index fibre of $([GeS_2]_{0.80}[Ga_2S_3]_{0.20})_{90}(CdI_2)_{10}$ composition is also provided in Fig. 9. The first observation concerns the mean level of attenuation, around 10-12 $dB.m^{-1}$ between 3 µm and 7 µm, which is similar for the two fibres even if some slight differences can be underlined. The intense and large absorption bands located around 4 µm and 6.6 µm for the two fibres are attributed to S-H and CS_2 vibrations, respectively. A less important absorption at 4.9 µm that originates from the C-S vibrations is also visible. Additional absorption bands are present for the step-index fibre. Concerning these differences, we can mention some slight supplementary peaks at 5.2 µm and 5.85 µm, for which the attribution is still under investigations and at 6.3 µm attributed to the molecular H_2O vibration.

These results are hopeful since although the core glass is heated two times no thermal deteriorations are observed. Moreover, in this step-index configuration the core of the fibre does not interact with the atmosphere. Consequently, the relative instability towards atmosphere that can occur for metal halide-based chalcogenide fibre is under control since the core of the fibre is surrounded by the clad. Indeed, at contrary to a mono-index fibre, the delivered power by the step-index fibre without any other protective polymer has been shown to be stable for several weeks.

Optical Materials EXPRESS

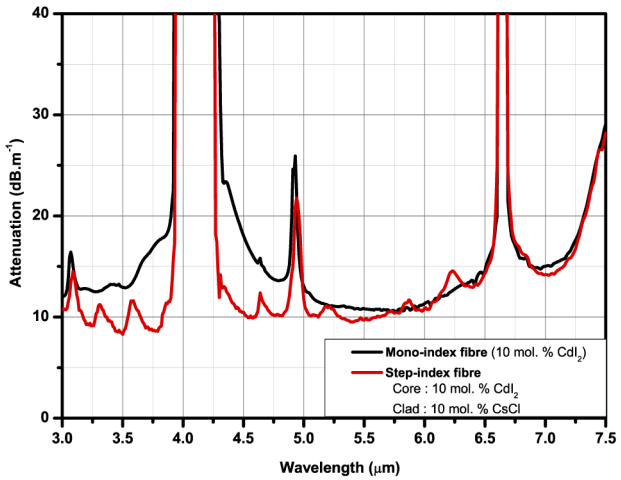


Fig. 9. Attenuation curve of the step-index fibre after removing the cladding modes (red). The black curve corresponds to the attenuation of a mono-index fibre having the same composition than the core of the step-index fibre.

5. Conclusions

Glasses based on the photowritable vitreous matrix GeS_2- Ga_2S_3, in which metal halide such as CsCl, CsI, $CdCl_2$, or CdI_2 is incorporated have been studied in order to have at disposal thermal and optical parameters for drawing a promising step-index fibre. The works have allowed to define a right core/clad combination to draw a multimode step-index fibre showing a minimal of 10 $dB.m^{-1}$ of losses for windows in the 3 µm - 7 µm range. Even if this result is very promising, for the future targeted applications, the optical losses have to be further reduced yet to positively consider a fibre laser effect once the earth-rare element will be inserted in the composition.

Funding

Agence de l'Innovation pour la Défense; Agence Nationale de la Recherche (ANR-17-CE24-0002-02).

Acknowledgment

The authors acknowledge both the French *Agence de l'Innovation pour la Défense* (AID) and the *Agence Nationale de la Recherche* (ANR, France) under Grant # ANR-17-CE24-0002-02 corresponding to the COMI project for their financial supports.

Disclosures

The authors declare that there are no conflicts of interest related to this article.

References

1. J. Lucas, J. Troles, X. H. Zhang, C. Boussard-Pledel, M. Poulain, and B. Bureau, "Glasses to See beyond Visible," C. R. Chim. **21**(10), 916–922 (2018).
2. V. S. Shiryaev and M. F. Churbanov, "Recent Advances in Preparation of High-Purity Chalcogenide Glasses for Mid-IR Photonics," J. Non-Cryst. Solids **475**, 1–9 (2017).
3. V. F. Kokorina, *Glasses for Infrared Optics* (CRC Press, (1996).
4. J. L. Adam, L. Calvez, J. Troles, and V. Nazabal, "Chalcogenide Glasses for Infrared Photonics," Int. J. Appl. Glass Sci. **6**(3), 287–294 (2015).

Optical Materials EXPRESS

5. P. Houizot, M. L. Anne, C. Boussard-Pledel, O. Loreal, H. Tariel, J. Lucas, and B. Bureau, "Shaping of Looped Miniaturized Chalcogenide Fibre Sensing Heads for Mid-Infrared Sensing," Sensors **14**(10), 17905–17914 (2014).
6. B. Xue, L. Calvez, M. Allix, G. Delaizir, and X. H. Zhang, "Amorphization by Mechanical Milling for Making IR Transparent Glass-Ceramics," J. Am. Ceram. Soc. **99**(5), 1573–1578 (2016).
7. M. Le Corvec, C. Boussard-Pledel, F. Charpentier, N. Fatih, B. Le Dare, F. Massart, F. Rojas, H. Tariel, O. Loreal, B. Bureau, J. Boustie, O. Sire, and F. Lohezic-Le Devehat, "Chemotaxonomic Discrimination of Lichen Species Using an Infrared Chalcogenide Fibre Optic Sensor: A Useful Tool for on-Field Biosourcing," RSC Adv. **6**(110), 108187 (2016).
8. P. Lucas, D. Le Coq, C. Juncker, J. Collier, and D. E. Boesewetter, "Evaluation of Toxic Agent Effects on Lung Cells by Fibre Evanescent Wave Spectroscopy," Appl. Spectrosc. **59**(1), 1–9 (2005).
9. K. Michel, B. Bureau, C. Boussard-Pledel, T. Jouan, J. L. Adam, K. Staubmann, and T. Baumann, "Monitoring of Pollutant in Waste Water by Infrared Spectroscopy Using Chalcogenide Glass Optical Fibres," Sens. Actuators, B **101**(1-2), 252–259 (2004).
10. M. L. Brandily, V. Monbet, B. Bureau, C. Boussard-Pledel, O. Loreal, J. L. Adam, and O. Sire, "Identification of Foodborne Pathogens within Food Matrices by IR Spectroscopy," Sens. Actuators, B **160**(1), 202–206 (2011).
11. K. Nagayam, M. Kakui, M. Matsui, I. Saitoh, and Y. Chigusa, "Ultra-Low-Loss (0.1484 dB/km) Pure Silica Core Fibre and Extension of Transmission Distance," Electron. Lett. **38**(20), 1168–1169 (2002).
12. T. Miya, Y. Terunuma, T. Hosaka, and T. Miyashita, "Ultimate Low-Loss Single-Mode Fibre at 1.55 µm," Electron. Lett. **15**(4), 106–108 (1979).
13. M. Meneghetti, C. Caillaud, R. Chahal, E. Galdo, L. Brilland, J. L. Adam, and J. Troles, "Purification of Ge-As-Se ternary glasses for the development of high quality microstructured optical fibers," J. Non-Cryst. Solids **503-504**, 84–88 (2019).
14. M. El-Amraoui, J. Fatome, J. C. Jules, B. Kibler, G. Gadret, C. Fortier, F. Smektala, I. Skripatchev, C. F. Polacchini, Y. Messaddeq, J. Troles, L. Brilland, M. Szpulak, and G. Renversez, "Strong Infrared Spectral Broadening in Low-Loss As-S Chalcogenide Suspended Core Microstructured Optical Fibres," Opt. Express **18**(5), 4547–4556 (2010).
15. Z. Yang, T. Luo, S. Jiang, J. Geng, and P. Lucas, "Single-Mode Low-Loss Optical Fibres for Long-Wave Infrared Transmission," Opt. Lett. **35**(20), 3360–3362 (2010).
16. S. Cherukulappurat, M. Guignard, C. Marchand, F. Smektala, and G. Boudebs, "Linear and Nonlinear Optical Characterization of Tellurium Based Chalcogenide Glasses," Opt. Commun. **242**(1-3), 313–319 (2004).
17. T. Cardinal, K. A. Richardson, H. Shim, A. Schulte, R. Beatty, K. Le Foulgoc, C. Meneghini, J. F. Viens, and A. Villeneuve, "Non-Linear Optical Properties of Chalcogenide Glasses in the System As–S–Se," J. Non-Cryst. Solids **256-257**, 353–360 (1999).
18. D. Marchese, M. De Sario, A. Jha, A. K. Kar, and E. C. Smith, "Highly Nonlinear GeS_2-Based Chalcohalide Glass for All-Optical Twin-Core-Fibre Switching," J. Opt. Soc. Am. B **15**(9), 2361–2370 (1998).
19. F. Starecki, A. Braud, N. Abdellaoui, J. L. Doualan, C. Boussard-Pledel, B. Bureau, P. Camy, and V. Nazabal, "7 to 8 µm Emission from Sm^{3+} Doped Selenide Fibres," Opt. Express **26**(20), 26462–26469 (2018).
20. M. C. Falcon, G. Palma, F. Starecki, V. Nazabal, J. Troles, S. Taccheo, M. Ferrari, and F. Prudenzano, "Design of an Efficient Pumping Scheme for Mid-IR Dy^{3+}:$Ga_5Ge_{20}Sb_{10}S_{65}$ PCF Fibre Laser," IEEE Photonics Technol. Lett. **28**(18), 1984–1987 (2016).
21. R. Chahal, F. Starecki, J. L. Doualan, P. Nemec, A. Trapanti, C. Prestipino, G. Tricot, C. Boussard-Pledel, K. Michel, A. Braud, P. Camy, J. L. Adam, B. Bureau, and V. Nazabal, "Nd^{3+}:Ga-Ge-Sb-S Glasses and Fibres for Luminescence in Mid-IR: Synthesis, Structural Characterization and Rare Earth Spectroscopy," Opt. Mater. Express **8**(6), 1650–1671 (2018).
22. L. Bodio, F. Starecki, J. Lemaitre, V. Nazabal, J. L. Doualan, E. Baudet, R. Chahal, A. Gutierrez-Arroyo, Y. Dumeige, I. Hardy, A. Braud, R. Soulard, P. Camy, P. Nemec, G. Palma, F. Prudenzano, and J. Charrier, "Mid-Infrared Guided Photoluminescence from Integrated Pr^{3+}-Doped Selenide Ridge Waveguides," Opt. Mater. **75**, 109–115 (2018).
23. B. McMillen, M. Li, S. Huang, B. Zhang, and K. P. Chen, "Ultrafast Laser Fabrication of Bragg Waveguides in Chalcogenide Glass," Opt. Lett. **39**(12), 3579–3582 (2014).
24. M. C. Falconi, G. Palma, F. Starecki, V. Nazabal, J. Troles, J. L. Adam, S. Taccheo, M. Ferrari, and F. Prudenzano, "Dysprosium-Doped Chalcogenide Master Oscillator Power Amplifier (MOPA) for Mid-IR Emission," J. Lightwave Technol. **35**(2), 265–273 (2017).
25. P. Masselin, E. Bychkov, and D. Le Coq, "Ultrafast Laser Inscription of High-Performance Mid-Infrared Waveguides in Chalcogenide Glass," IEEE Photonics Technol. Lett. **30**(24), 2123–2126 (2018).
26. C. Florea, J. S. Sanghera, and I. D. Aggarwal, "Direct-Write Gratings in Chalcogenide Bulk Glasses and Fibres Using a Femtosecond Laser," Opt. Mater. **30**(10), 1603–1606 (2008).
27. O. Caulier, D. Le Coq, E. Bychkov, and P. Masselin, "Direct Laser Writing of Buried Waveguide in As_2S_3 Glass Using a Helical Sample Translation," Opt. Lett. **38**(20), 4212–4215 (2013).
28. P. Masselin, E. Bychkov, and D. Le Coq, "Direct Laser Writing of a Low-Loss Waveguide with Independent Control over the Transverse Dimension and the Refractive Index Contrast between the Core and the Cladding," Opt. Lett. **41**(15), 3507–3510 (2016).
29. A. Brehault, L. Calvez, P. Adam, J. Rollin, M. Cathelinaud, B. Fan, O. Merdrignac-Conanec, T. Pain, and X. H. Zhang, "Moldable Multispectral Glasses in GeS_2–Ga_2S_3–CsCl System Transparent from the Visible up to the Thermal Infrared Regions," J. Non-Cryst. Solids **431**, 25–30 (2016).

Optical Materials EXPRESS

30. G. Fuxi, M. Xilai, Z. Mingli, and Y. Peihong, "Study on Ge-Ga-X (X = S, Se) glass systems," *Journal of The Chinese Ceramic Society* (1987).
31. I. Pethe, V. Nazabal, R. Chahal, B. Bureau, I. Kaban, S. Belin, and P. Jovari, "Local Motifs in GeS_2–Ga_2S_3 Glasses," J. Alloys Compd. **673**, 149–157 (2016).
32. Y. Ledemi, L. Calvez, M. Roze, X. H. Zhang, B. Bureau, M. Poulain, and Y. Messaddeq, "Totally Visible Transparent Chloro–Sulphide Glasses Based on Ga_2S_3 – GeS_2 – CsCl," *Journal of Optoelectronics and Advanced Materials*, 6 (2007).
33. P. Masselin, D. Le Coq, A. Cuisset, and E. Bychkov, "Spatially Resolved Raman Analysis of Laser Induced Refractive Index Variation in Chalcogenide Glass," Opt. Mater. Express **2**(12), 1768–1775 (2012).
34. G. Tao, H. Ebendorff-Heidepriem, A. M. Stolyarov, S. Danto, J. V. Badding, Y. Fink, J. Ballato, and A. F. Abouraddy, "Infrared Fibres," Adv. Opt. Photonics **7**(2), 379–458 (2015).
35. P. Houizot, C. Boussard-Pledel, A. J. Faber, L. K. Cheng, B. Bureau, P. A. Van Nijnatten, W. L. M. Gielesen, J. Pereira do Carmo, and J. Lucas, "Infrared Single Mode Chalcogenide Glass Fibre for Space," Opt. Express **15**(19), 12529–12538 (2007).
36. Y. Ledemi, B. Bureau, L. Calvez, M. Le Floch, M. Roze, C. Lin, and X. H. Zhang, "Structural Investigations of Glass Ceramics in the Ga_2S_3–GeS_2–CsCl System," J. Phys. Chem. B **113**(44), 14574–14580 (2009).
37. R. T. Kersten, "A New Method for Measuring Refractive Index and Thickness of Liquid and Deposited Solid Thin Films," Opt. Commun. **13**(3), 327–329 (1975).
38. K. Jinguj, M. Horiguchi, and T. Manabe, "Spectral Loss Measurement System for IR Optical Fibres," Appl. Opt. **21**(4), 571–572 (1982).
39. A. Tverjanovich, Y. S. Tver'yanovic, and S. Loheider, "Raman Spectra of Gallium Sulfide Based Glasses," J. Non-Cryst. Solids **208**(1-2), 49–55 (1996).
40. Yu. S. Tver'yanovic, V. V. Aleksandrov, I. V. Murin, and E. G. Nedoshovenko, "Glass-Forming Ability and Cationic Transport in Gallium Containing Chalcohalide Glasses," J. Non-Cryst. Solids **256-257**, 237–241 (1999).
41. Yu. S. Tver'yanovic, M. Vlcek, and A. Tverjanovich, "Formation of Complex Structural Units and Structure of Some Chalco-Halide Glasses," J. Non-Cryst. Solids **333**(1), 85–89 (2004).
42. A. Cuisset, F. Hindle, J. Laureyns, and E. Bychkov, "Structural Analysis of $XCsCl(1-x)Ga_2S_3$ Glasses by Means of DFT Calculations and Raman Spectroscopy," J. Raman Spectrosc. **41**(9), 1050–1058 (2010).
43. P. Masselin, D. Le Coq, L. Calvez, E. Petracovschi, E. Lepine, E. Bykov, and X. H. Zhang, "CsCl effect on the optical properties of the $80GeS_2$–$20Ga_2S_3$ base glass," Appl. Phys. A **106**, 697–702 (2010).
44. B. Frumarova, J. Oswald, P. Krecmer, M. Frumar, V. Cerny, and V. Smrcka, "Synthesis and Physical Properties of the System $(GeS_2)80-x(Ga_2S_3)20$:xPr Glasses," Opt. Mater. **6**(3), 217–223 (1996).
45. A. Boskovic, S. V. Chernikov, J. R. Taylor, L. Gruner-Nielsen, and O. A. Levring, "Direct Continuous-Wave Measurement of n_2 in Various Types of Telecommunication Fibre at 1.55 μm," Opt. Lett. **21**(24), 1966–1968 (1996).
46. J. Troles, F. Smektala, G. Boubebs, A. Monteil, B. Bruneau, and J. Lucas, "Chalcogenide glasses as solid state optical limiters at 1.064 μm," Opt. Mater. **25**(2), 231–237 (2004).

88.253.47.212 {ts '2021-05-28 05:06:11'}